Estimation of Snow and Firn Properties by means of Multi-Angular Polarimetric SAR Measurements

Giuseppe Parrella, German Aerospace Center (DLR), giuseppe.parrella@dlr.de, Germany
Irena Hajnsek, German Aerospace Center (DLR), irena.hajnsek@dlr.de, Germany & ETH Zurich, Switzerland
Konstantinos P. Papathanassiou, German Aerospace Center (DLR), kostas.papathanassiou@dlr.de, Germany

Abstract

The retrieval of snow and firn properties on large scales is essential for a wide range of cryosphere applications and research questions, implying the necessity to employ remote sensing. Among the existing remote sensing techniques, synthetic aperture radars (SARs) allow monitoring polar regions independently of sun illumination and in (nearly) all-weather conditions. The penetration capability of microwave into dry snow, firn and ice makes SAR measurements sensitive to the internal structure of snow and ice layers. In this study, a physical model is explored to assess the potential to retrieve snow and firn properties, such as layer depth, density and anisotropy, from multi-angular polarimetric SAR measurements. The experimental validation is carried over the Austfonna ice cap, in Svalbard, using ALOS-2 PALSAR-2 data.

1 Introduction

The potential of polarimetric SAR for the monitoring of snow, firn and ice properties is recognised since the early 1990s [1]. Since then, a number of applications has been established, like the discrimination of wet and dry snow, and the snow melt onset detection based on polarimetric data [2]. Regarding land ice, the relation between multi-polarization backscattering coefficients and the seasonal changes of some Arctic glaciers was already investigated in [3]. More recently, a technique based on statistical modeling of polarimetric covariance matrices was proposed to map the firn line position on a glacier in Svalbard [4]. Finally, recent studies have clearly shown that information concerning firn and snow properties is also contained in the phase difference measured between the two co-polarization (co-pol) channels (HH and VV) [5][6]. The physical model proposed in [5] establishes a link between co-pol phase differences (CPDs) and the depth, density and structural anisotropy of firn layers. Similarly, the model in [6] provides an interpretation of co-pol phase differences for a snow-over-ground scenario in terms of fresh snow properties. However, both models lead, for a single polarimetric measurement, to an under-determined system as they describe a single observable (the CPD) as a function of three parameters (depth, density and structural anisotropy). Up to now, the problem has been balanced by using external information about two of the three parameters, as shown in [5] and [6]. However, this is a rare case since ground measurements of snow/firn properties can only be collected over very small areas. For larger areas, the under-determination of the problem can be addressed by expanding the observation space. One option is to explore polarimetric measurements performed at different incidence angles. The objective of this study is to investigate the possibility of a joint retrieval of snow/firn depth, density and anisotropy by extending the two approaches in [5] and [6] to the case of multi-angular polarimetric SAR measurements.

2 Model for Polarimetric Phase Differences

Only the model in [5] that relates CPDs to firn properties is recalled here and reviewed with respect to its suitability for a multi-angular inversion. In the case of snow, the model in [6] can be extended in a similar way. The CPD is defined as:

$$CPD = \phi_{\text{HH}} - \phi_{\text{VV}}, \qquad (1)$$

where ϕ_{HH} and ϕ_{VV} are the phase terms of the HH and VV channel, respectively. According to the model in [5], positive CPD values can result from the propagation of the radar signal through firn layers, which are typically characterized by a vertical structural (and dielectric) anisotropy. The model describes the CPD as a function of the firn depth l, the permittivity components in the direction of the horizontal and vertical polarization, ε_h and ε_v respectively, the refracted radar incidence angle ϑ_r and the wavelength λ_0 [5]:

$$CPD = \angle\left\{\int_0^l \sigma(z) e^{2j\frac{2\pi}{\lambda_0}(\sqrt{\varepsilon_v} - \sqrt{\varepsilon_h})\frac{z}{\cos\vartheta_r}} dz\right\}, \quad (2)$$

where the term $\sigma(z)$ is additionally introduced to account for the vertical distribution of the scatterers embedded in the firn layer. The permittivity components are functions of the structural anisotropy, which determines the dielectric anisotropy $\Delta\varepsilon = \varepsilon_v - \varepsilon_h$, and of the firn density (ρ). It is important to point out that the depth l does not necessarily correspond to the entire thickness of the firn layer present in the imaged area. It rather refers to the depth of the layer sensed by the radar, which corresponds to the penetration depth of the signal if the latter is smaller than the thickness of the entire firn volume.

The *CPD* in (2) is proportional to depth, so that larger phase differences are associated to thicker firn layers. For a given depth, the *CPD* increases with $\Delta\varepsilon$ as the H and V polarized signals propagate through an increasingly anisotropic medium. Contrarily, the modelled *CPD* is inversely proportional to density, at least in the typical range of values applicable to firn (0.4-0.8 g/cm^3), as the effect of the anisotropic structure tends to disappear when the firn volume becomes denser [5]. Overall, the model in (2) leads to an under-determined problem with a single equation and three (firn) parameters. The inversion of any of such quantities requires the knowledge of the other two.

Beside the firn properties, the *CPD* also depends on the wavelength and the incidence angle of the imaging SAR. This second case is of main interest, since most current sensors are able to perform measurements at different incidence angles, which can be exploited to extend the observation space.

2.1 Dependency on incidence angle

In (2), the dependency of the *CPD* on the (refracted) incidence angle ϑ_r results in larger phase differences at grazing incidence angles, for given values of depth and density, as shown in [5]. This is essentially related to two factors: first, the dielectric anisotropy is only in the vertical direction and, therefore, it becomes more effective when the V polarization tends to align parallel to such direction (i.e. for $\vartheta \rightarrow 90°$); second, the optical path into the anisotropic layer increases with ϑ, so that the radar signal experiences differential propagation for a longer path. Figure 1 shows the modelled *CPD* obtained for identical model settings, except for a variation of the incidence angle from 30°, in the first case, to 35° in the second one. The wavelength of the radar signal is fixed to $\lambda = 0.23$ m and the firn density to $\rho = 0.6$ g/cm^3. The dielectric anisotropy is allowed to vary in a range of values typical for firn [7], between $\Delta\varepsilon = 0.02$ and $\Delta\varepsilon = 0.07$ (colored lines), while a depth range from 0 m to 10 m is considered. As mentioned above, the increase of ϑ from 30°(top panel of Figure 1) to 35° (mid panel) determines a general increase of the *CPD* (ΔCPD), depicted in the bottom panel of Figure 1.
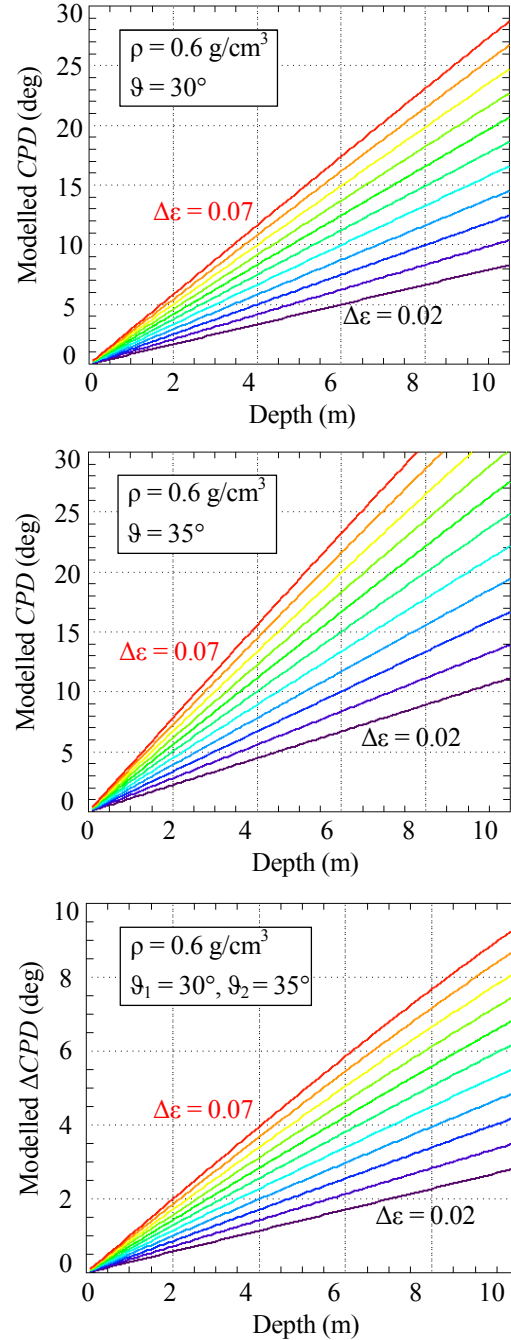

Figure 1: Top and mid panel - Simulated *CPD* as a function of depth, for a layer of anisotropic firn of density 0.6 g/cm^3 and dielectric anisotropy $\Delta\varepsilon$ ranging from 0.02 (black line) to 0.07 (red), with 0.005 spacing. The radar wavelength is fixed to λ=0.23 m (L-band), and the incidence angle to ϑ=30° (top panel) and ϑ=35° (bottom). Bottom panel – Difference of *CPD* obtained for the case of ϑ=35° and ϑ=30°.

As expected, the ΔCPD is proportional to both depth and $\Delta\varepsilon$. For instance, assuming a depth of 5 m, the CPD increases slightly more than 1° if $\Delta\varepsilon = 0.02$, while a difference of around 5° is predicted if $\Delta\varepsilon = 0.07$. Such

behaviour can be exploited for a joint retrieval of l and $\Delta\varepsilon$ based on two CPD measurements performed with two different incidence angles over a given area.

The simulations shown in Figure 1 refer to an arbitrary value of density. However, ρ is an unknown model parameter which also needs to be retrieved if not provided by external information. The assumption of a too high (respectively, too low) value of ρ leads to overestimation (underestimation) of l and $\Delta\varepsilon$. Similarly to the previous case, the angular dependency of the *CPD* in (2) can be exploited to further expand the observation space and attempt the joint retrieval of the three firn parameters – l, $\Delta\varepsilon$ and ρ – based on three *CPD* measurements performed at three different ϑ.

2.2 Multi-angular model inversion

Angular diversity allows to expand the observation space from 1 to 3 measurements, allowing to balance the number of observables and unknowns in (2). However, it is known that the penetration depth (that is the depth to be retrieved) can vary with the incidence angle. This could lead to an increase of the number of parameters, i.e. unknowns, in the retrieval. In the case of three different incidence angles, the problem can be described by 3 equations and 5 parameters $(l_1, l_2, l_3, \rho, \Delta\varepsilon)$:

$$\begin{cases} CPD_1 = f_1(l_1, \rho, \Delta\varepsilon) & \vartheta = \vartheta_1, \\ CPD_2 = f_2(l_2, \rho, \Delta\varepsilon) & \text{for} \quad \vartheta = \vartheta_2, \\ CPD_3 = f_3(l_3, \rho, \Delta\varepsilon) & \vartheta = \vartheta_3. \end{cases} \quad (3)$$

where l_1, l_2, l_3 are the three penetration depths at the different incidence angles. Nevertheless, it is reasonable to assume that the penetration depth is the same if the three values of ϑ do not differ more than very few degrees from each other. In this case, $l_1 = l_2 = l_3 = l$ and the system is well-determined. Under this assumption, it becomes possible to jointly invert the 3 unknown firn properties from the 3 *CPD* measurements.

3 Experiments with real data

3.1 Test site and available SAR data

Preliminary tests of the proposed multi-angular approach have been performed using polarimetric ALOS-2 PALSAR-2 data acquired over the Austfonna ice cap, in Svalbard. In total, 7 acquisitions are available from the winter 2016/2017 (December-April), with incidence angle ranging from 27.8° to 36.5° and spatial resolution of 5 m x 3 m (range x azimuth). Figure 2 shows a mosaic of the *CPD* extracted from the data with an estimation window size of approximately 70 m x 70 m. The firn zone can be easily identified in the inner area of the ice cap, which exhibits positive *CPD* values.

Interestingly, the transition between two adjacent scenes is also clearly visible if the respective incidence angles differ significantly. This is, for instance, the case of the scenes marked by the red and green boxes, acquired on 04/01/2017 with $\vartheta = 33.9°$ and on 23/03/2017 with $\vartheta = 27.8°$, respectively.

3.2 Preliminary results

A first test of the proposed approach has focused on the portion of firn zone covered by both scenes. As only two incidence angles are available in this case, the joint retrieval could be tested at this stage only for two parameters. A first assessment of the benefit of the proposed procedure has been performed by comparing the firn depth map obtained when the joint estimation of $\Delta\varepsilon$ is performed, with the firn depth map retrieved assuming an arbitrary value of $\Delta\varepsilon$.
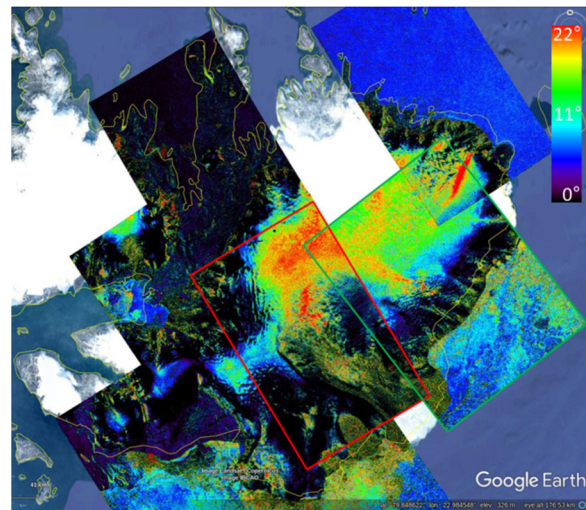

Figure 2: *CPD* mosaic over the Austfonna ice cap extracted from the available ALOS-2 SAR data.

In the case of the joint retrieval of l and $\Delta\varepsilon$, a density value of $\rho = 0.6$ g/cm^3 has been considered, while the additional assumption of $\Delta\varepsilon = 0.04$ has been made to perform the inversion in the other case. Figure 3 shows the firn depth maps obtained with the two approaches. The map obtained from single-angle *CPD* measurements (top panel) clearly points out how the assumption of an arbitrary $\Delta\varepsilon$ can lead to unrealistic values of l, as the estimates are strongly dependent on the incidence angle. For instance, discrepancies up to 5 m are found for overlapping pixels in the two SAR scenes. The bottom panel of Figure 3 shows the map obtained when the joint estimation is performed. In particular, the procedure is applied to the area of overlap, providing a map of depth and dielectric anisotropy (not shown here). As the joint estimation is only possible over such limited area, the mean of the $\Delta\varepsilon$ estimates is used to perform the inversion of the firn depth over the remaining areas in the two scenes.
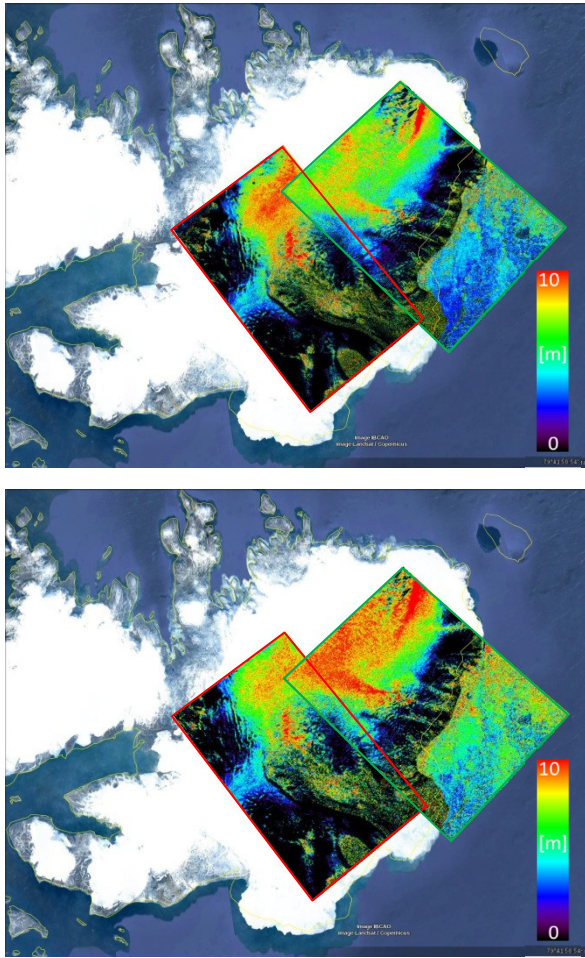
Figure 3: Top – firn depth map obtained from single-angle *CPD* measurements with the assumption of $\Delta\varepsilon = 0.04$; bottom – firn depth estimated jointly with $\Delta\varepsilon$ using the proposed multi-angular approach.

The joint estimation provides a mean $\Delta\varepsilon = 0.045$ and, in general, significantly more consistent depth values at the transition between the two scenes. This confirms the benefit of exploiting the additional information provided by the angular diversity as this allows $\Delta\varepsilon$ to be estimated from the data instead of assumed a-priori. The temporal separation (around 2.5 months) between the two acquisitions is expected to have a negligible impact in terms of possible changes in the firn properties, as long as both scenes are taken during the same winter season and dry snow conditions are verified throughout the period. Further tests will be conducted on areas imaged with three different incidence angles to assess the full potential of the joint retrieval of firn depth, density and dielectric anisotropy based on polarimetric SAR data.

References

[1] H. Rott and R. Davies, "Multifrequency and polarization SAR observations of alpine glaciers," Ann. Glaciol., 17, 98-104, 1993.

[2] T. Nagler, H. Rott, E. Ripper, G. Bippus and M. Hetzenecker, "Advancements for snowmelt monitoring by means of Sentinel-1 SAR," Remote Sens., 8(4), 348, 2016.

[3] R. V. Engeset, J. Kohler, K. Melvold and B. Lundèn, "Change detection and monitoring of glacier mass balance and facies using ERS SAR winter images over Svalbard," Int. J. Remote Sens., 3(10), 2023-2050, 2002.

[4] V. Akbari, A. Doulgeris and T. Eltoft, "Monitoring glacier changes using multitemporal multipolarization SAR images", IEEE Trans. Geosci. Remote Sens., 52(6), 3729-3741, Jun. 2014.

[5] G. Parrella, I. Hajnsek and K. Papathanassiou, "Polarimetric decomposition of L-band PolSAR backscattering over the Austfonna ice cap", IEEE Trans. Geosci. Remote Sens., 54(3), 1267-1281, Mar. 2016.

[6] S. Leinss, G. Parrella and I. Hajnsek, "Snow height determination by polarimetric phase differences in X-band SAR data", IEEE J. Sel. Topics Appl. Earth Observ. Remote Sens., 7(9), 3794-3810, Jun. 2014.

[7] S. Fujita, M. Hirabayashi, K. Goto-Azuma, R. Dallmayr, K. Satow, J. Zheng and D. Dahl-Jensen, "Densification of layered firn on the ice sheet at NEEM, Greenland", J. Glaciol., 60(223), 905-921, 2014.